J. CHEM. SOC. FARADAY TRANS., 1992, 88(4), 525–529

Observation of Perturbations in the Rotational Manifold of the CN B $^2\Sigma^+$ $v = 1$ Level caused by Interaction with the CN A $^2\Pi_i$ $v = 12$ Level

J. F. Black† and R. N. Zare*
Department of Chemistry, Stanford University, Stanford, California 94305-5080 USA

The (1, 0) band of the CN B $^2\Sigma^+$–X $^2\Sigma^+$ transition has been examined using sub-Doppler laser-induced fluorescence (LIF), and the spin–rotation splitting of the upper state was found to vary irregularly. This behaviour is identified as arising from localised perturbations of the CN B $^2\Sigma^+$ ($v = 1$) level caused by interaction with levels of the same total angular momentum arising from the $v = 12$ vibrational level of the A $^2\Pi_i$ state. A deperturbation analysis based on diagonalising the Hamiltonian of the B $^2\Sigma^+$ and A $^2\Pi_i$ states including their mutual interaction is able to match well the experimentally observed separations between the $F_1(J = N + \frac{1}{2})$ and $F_2(J = N - \frac{1}{2})$ levels of the B $^2\Sigma^+$ state.

The CN B $^2\Sigma^+$–X $^2\Sigma^+$ system (the violet band system) has been the subject of intense scrutiny for many years.[1–9] The transition itself has become a classic textbook example of a $^2\Sigma$–$^2\Sigma$ transition while extra interest stems from the highly visible and theoretically tractable interaction of the levels of the B $^2\Sigma^+$ state with high-lying rovibrational levels of the A $^2\Pi_i$ state.

The CN B–X transition has also found favour as a probe of the internal quantum state distribution of CN (X $^2\Sigma^+$) radicals formed in a variety of chemical dynamics experiments. In particular, the photodissociation of the family of cyanogen halides has become a benchmark against which theories are tested and new experiments proved.[10–21] Our own interest here stems from the photodissociation process

$$\mathrm{ICN} + h\nu(249\ \mathrm{nm}) \rightarrow \mathrm{CN}\ \mathrm{X}\ ^2\Sigma^+(v, N) + \mathrm{I}(^2\mathrm{P}_{1/2,3/2})$$

which has been under extensive study in this laboratory for some time.[16–21] Of particular interest are the ongoing efforts to understand the non-adiabatic forces acting in the dissociation, which manifest themselves in the most detailed experimental studies. In the course of making these measurements on the (1, 0) band of the B–X system, we have identified a perturbation in the rotational manifold of the $v = 1$ level of the B state. Our experiments are sensitive to the spin–rotation splitting of the N levels in the B $^2\Sigma^+$ state, and we observe the perturbation as a non-monotonically varying value of the effective spin–rotation doubling constant γ'_{eff} for the $v = 1$ level of the B state.

The experimental values of the $F_1(J = N + \frac{1}{2})$ and $F_2(J = N - \frac{1}{2})$ spin–rotation doublet level separation obtained from these values of γ'_{eff} are compared with those calculated by diagonalising the Hamiltonian matrix representing the $^2\Sigma$–$^2\Pi_i$ interaction. The existing body of spectroscopic data on the CN A–B interaction is found to reproduce well the effects observed here.

Experimental

Fig. 1 shows a schematic diagram of the experimental apparatus, which has been discussed extensively elsewhere.[20] Briefly, the output of an excimer laser (Lumonics TE 860-2) is divided into two equal parts. One beam is recollimated, irised down and polarised to form the photolysis beam. This is directed into the vacuum system *via* extensively baffled arms, which are also equipped with an argon purge. This purge helps counter the build-up of photolysis debris on the windows and serves to reduce absorption of the 249 nm photons by the ICN before the scattering region is reached. Typical powers are $\leqslant 850$ μJ per pulse in an 8 mm diameter spot.

The other excimer beam pumps a dye laser (Lambda Physik FL2002E) operating at *ca.* 358 nm or greater (PBD dye, Exciton in cyclohexane). This wavelength is resonant with the (1, 0) transition in the B–X system.[20] The beam is sent round an optical delay line, is polarised and then directed into the vacuum system *via* extensively baffled arms. The pulse arrives at the scattering centre *ca.* 35 ns after the photolysis pulse. We observe the nascent CN photofragment distribution at partial pressures of Ar (10 mTorr) and ICN (2–10 mTorr). Typical powers for the dye laser are 100–400 nJ per pulse in a 6 mm diameter spot.

The photolysis and probe beams are monitored by photodiodes (Hamamatsu S1336-5BQ) coupled to a sample-and-hold circuit built in-house. An etalon (Virgo ET-100) is used to monitor the dye laser linewidth and provide a standard against which to linearise the frequency abscissae of the sub-Doppler spectra generated. The dye laser is pressure-tuned using filtered dry nitrogen.

LIF photons are collected along the direction normal to the plane containing the photolysis- and probe-beam wavevectors. A single lens (1.5″ diameter, $f = 60$ mm) in the vacuum chamber collects the fluorescence and focuses it onto the photocathode of a photomultiplier tube (RCA 7326). The output is amplified and digitised for >120 ns (*ca.* 2 lifetimes[1]). Data are normalised to the pump and probe laser powers. ICN (Kodak) flows through the chamber as a vapour (2–10 mTorr). There is no evidence of memory effects from previous laser pulses or impurities.

Results

Broad-band Spectra

Fig. 2 shows a portion of the fluorescence excitation spectrum of the R branch of the B–X (1, 0) band. The minor features are the R branches of the (2, 1), (3, 2) and (4, 3) bands of the same electronic system. The eye is immediately drawn to the perturbation at $N'' = 45$, evidenced by the complete resolution of the two spin–rotation doublets of this line. This spectrum was taken under broad-band conditions, with no etalon in the dye laser cavity.

† SERC/NATO post-doctoral fellow 1987–1989. Present address: Department of Chemistry, Columbia University, New York, NY 10027, USA.

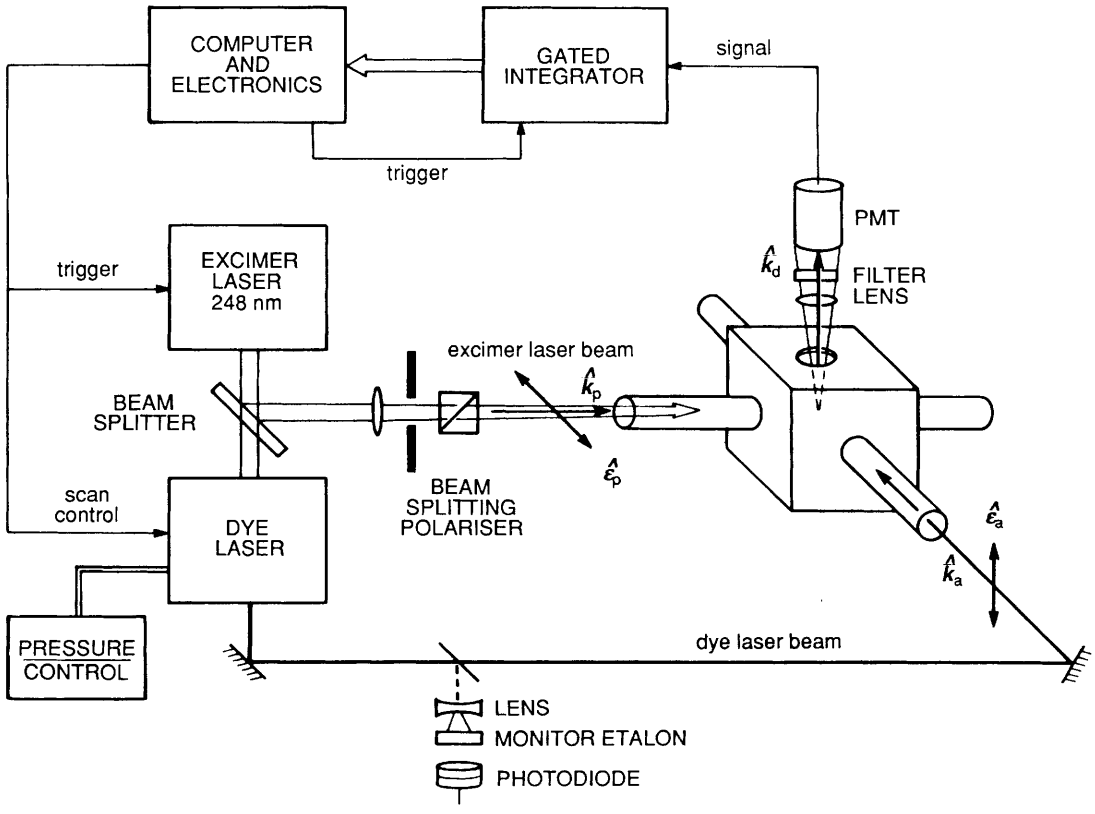

Fig. 1 Schematic diagram of the apparatus used in the CN Doppler profile experiments

Sub-Doppler Spectra

Fig. 3 shows a high-resolution fluorescence excitation spectrum of the R(53) line in the B–X (1, 0) band. The integrated intensity of the line has been normalised to 1 for the purposes of fitting. The dye laser linewidth here is $\leqslant 0.06$ cm^{-1}. The complicated appearance of the line arises from a combination of (*a*) partial spectroscopic resolution of the F_1 ($J = N + \frac{1}{2}$) and F_2($J = N - \frac{1}{2}$) components and (*b*) a large and highly anisotropic energy release in the photodissociation giving Doppler-broadened lines with characteristic shapes.[20] Our choice of experimental geometry emphasises the latter point. The solid line is the result of fitting the data to a standard model.

We have studied R-branch members of the CN B–X (1, 0) band without underlying lines from the (2, 1), (3, 2) and (4, 3) bands. Those with underlying lines show asymmetries that make them difficult to fit and, in view of the complications already present in the system,[20] we choose to ignore them.

Analysis of Doppler Profiles

The method of analysis has been discussed extensively elsewhere.[20] Briefly, an LIF lineshape, in the absence of aniso-

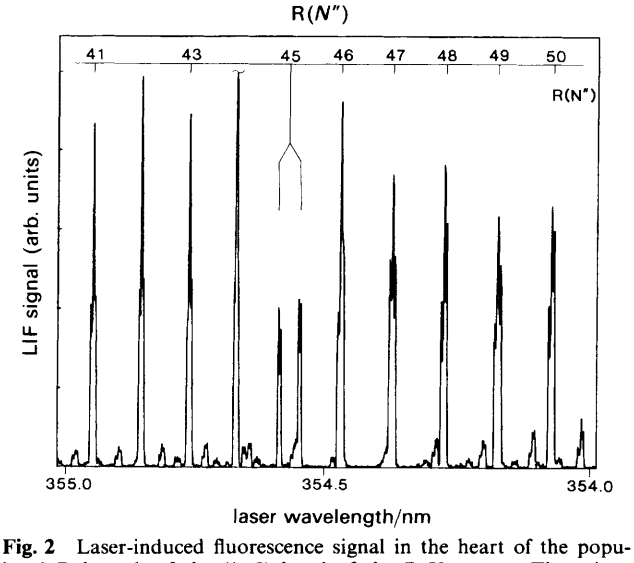

Fig. 2 Laser-induced fluorescence signal in the heart of the populated R branch of the (1, 0) band of the B–X system. The minor features are the (2, 1), (3, 2) and (4, 3) bands. Note the dramatic effect of state interaction at $N' = 46$. The spin–rotation splitting, unresolvable in the other lines of the spectrum, has widened to *ca.* 3.347 cm^{-1}

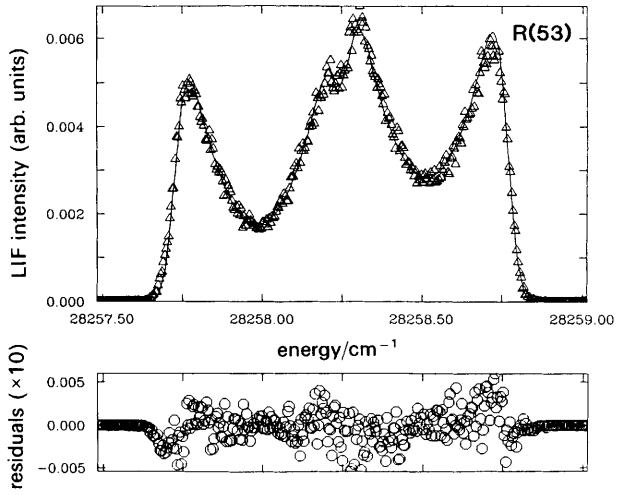

Fig. 3 High-resolution fluorescence excitation spectrum of the R(53) line of the CN B–X (1, 0) band. The solid line is a fit to a model using eqn. (1) to the data (△). Residuals from the fit (○) are shown in the lower panel, plotted at a scale × 10 of that of the main spectrum. The energy scale is in vacuum wavenumbers

tropic motion and assuming a delta-function laser linewidth, can be well represented as a rectangular (top-hat) shape with width $2v_0\, v/c$, where v_0 is the natural transition frequency, v is the speed of the target (assuming a monochromatic isotropic velocity distribution) and c is the speed of light. Usually, the effects of a non-negligible laser linewidth and polychromatic target motion are taken into account by folding the 'top-hat' with Gaussians, calculated to reproduce the effects of linewidth and motion. The problems associated with non-isotropic motion in the laboratory frame have also been discussed elsewhere in great detail.[22–38] Again briefly, we have

$$I(\theta) = \frac{1}{4\pi}\,[1 + \beta P_2(\cos\theta)] \qquad (1)$$

where $I(\theta)$ is the differential cross-section for photofragments scattering into the differential solid angle element $\sin\theta\, d\theta\, d\phi$ and where θ is the angle subtended by the photolysis beam electric vector $\boldsymbol{\varepsilon}_p$ and the fragment recoil velocity vector $\boldsymbol{v}$. Here $P_2(\cos\theta)$ is the second Legendre polynomial in $\cos\theta$ and β is the dimensionless anisotropy parameter, which has boundary values $-1 \leqslant \beta \leqslant 2$. Fig. 4 of the paper of Hall *et al.*[36] nicely illustrates the effect of anisotropic energy release on LIF lineshapes, given various experimental geometries and dissociation mechanisms. Our original study[20] involved fitting the lineshapes of a number of LIF transitions in the R branch of the (1, 0) band to expressions of the form of eqn. (1).

During the course of the analysis, we realised that the splitting between the two spin–rotation doublet components, given roughly as[1]

$$\Delta\nu_{F_1,F_2} = (\gamma' - \gamma'')N'' + \tfrac{1}{2}(3\gamma' - \gamma'') \qquad (2)$$

did not vary linearly and monotonically with N'', as eqn. (2) would suggest. (Note that the effects of line broadening caused by energy release, line profile from anisotropy and line splitting from spin–rotation doubling can all be reliably separated.[20]) We have developed the analysis by fitting the line profiles to an effective upper-state spin–rotation doubling constant, $\gamma'_{\rm eff}$. Fig. 4 shows a plot of $\gamma'_{\rm eff}$ *vs.* N' for the values of N' analysed.

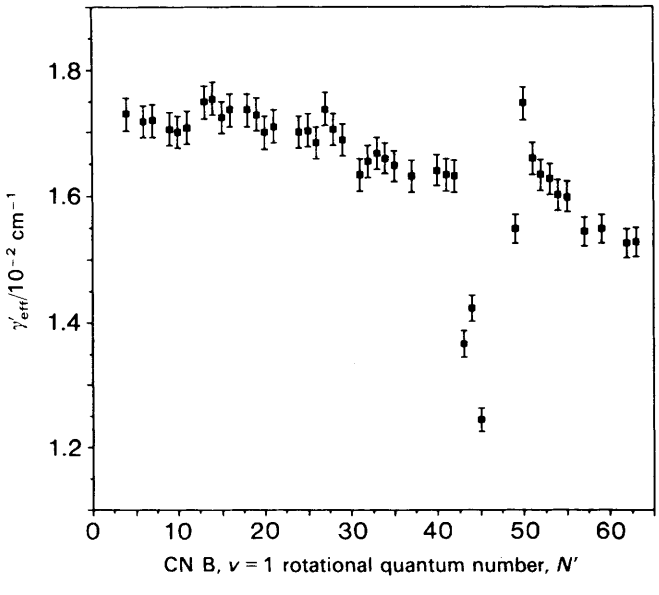

Fig. 4 A plot of the effective spin–rotation interaction constant ($\gamma'_{\rm eff}$) for the $v = 1$ level of the CN $B\,^2\Sigma^+$ state. Error bars represent the latitude beyond which *gross* deterioration of the fit was observed

Between three and six spectra were analysed for each value of N'. Note the effects of the perturbation around $N' = 43$–50. The value for $N' = 46$ is considerably off-scale in this plot, which is estimated using eqn. (2) to be *ca.* 7.72×10^{-2} cm^{-1}. The mean numerical values are given in Table 1. Lines not analysed are contaminated by underlying transitions. The error bars on the plot represent the latitude beyond which gross deterioration of the fit occurred, as determined by trial and inspection. In most cases, the error is around $\pm 1.5\%$ of the actual value.

The overall trend to less positive values with increasing N' may be explained by considering the first-order centrifugal distortion correction to the spin–rotation doubling constant, γ_D. Ito *et al.*[8] have shown that for the B state, $v = 1$ rotational manifold, this takes the value of -5.0×10^{-7} cm^{-1}. For $N' = 60$, this yields a corrected value for $\gamma'_{\rm eff}$ of *ca.* 1.53×10^{-2} cm^{-1}, in good agreement with the observations made here.

The experimental spin–rotation splitting is calculated using the form of eqn. (2) incorporating higher-order terms for the ground state. These experimental values are then compared with those calculated according to theory.

Theoretical Analysis

Following Ito *et al.*,[8] the Hamiltonian matrix describing the $B\,^2\Sigma^+$–$A\,^2\Pi_i$ interaction is assembled from the elements

$$\begin{aligned} H(^2\Sigma^+, {}^2\Sigma^+) = {} & E_\Sigma + B_\Sigma x(x \pm 1) - D_\Sigma x^2(x \pm 1)^2 \\ & + H_\Sigma X^3(x \pm 1)^3 - \tfrac{1}{2}(1 \pm x) \\ & \times [\gamma_\Sigma + \gamma_{D\Sigma} N(N+1) + \gamma_{H\Sigma} N^2(N+1)^2] \end{aligned} \qquad (3)$$

$$\begin{aligned} H(^2\Pi_{1/2}, {}^2\Pi_{1/2}) = {} & E_\Pi + B_\Pi x^2 - D_\Pi(x^4 + x^2 - 1) \\ & + H_\Pi(x^6 + 3x^4 - 5x^2 + 2) \\ & - \tfrac{1}{2}A_\Pi + A_{D\Pi} x^2 \\ & + \tfrac{1}{2}(1 \pm x)[p_\Pi + q_\Pi(1 \pm x)] \end{aligned} \qquad (4)$$

$$\begin{aligned} H(^2\Pi_{3/2}, {}^2\Pi_{3/2}) = {} & E_\Pi + B_\Pi(x^2 - 2) - D_\Pi(x^4 - 3x^2 + 3) \\ & + H_\Pi(x^6 - 3x^4 + 5x^2 - 4) \\ & + \tfrac{1}{2}A_\Pi + A_{D\Pi}(x^2 - 2) + \tfrac{1}{2}q_\Pi(x^2 - 1) \end{aligned} \qquad (5)$$

$$\begin{aligned} H(^2\Pi_{1/2}, {}^2\Pi_{3/2}) = {} & -B_\Pi(x^2 - 1)^{1/2} + 2D_\Pi(x^2 - 1)^{3/2} \\ & - H_\Pi(x^2 - 1)^{1/2}(3x^4 - 5x^2 + 3) \\ & - \tfrac{1}{4}(x^2 - 1)^{1/2}[p_\Pi + 2q_\Pi(1 \pm x)] \end{aligned} \qquad (6)$$

$$H(^2\Sigma^+, {}^2\Pi_{1/2}) = \alpha + \beta(1 \pm x) \qquad (7)$$

and

$$H(^2\Sigma^+, {}^2\Pi_{3/2}) = -\beta(x^2 - 1)^{1/2} \qquad (8)$$

calculated using the method of Zare *et al.*[39] Here the lower portions of the $\pm$ signs correspond to the levels of e parity, $N = J - \frac{1}{2} = x - 1$, and the upper signs to the f parity levels, $N = J + \frac{1}{2} = x$. The terms E, A, B, D ... have their usual spectroscopic meaning. The α and β terms are, respectively, the constants parametrising the spin–orbit and rotation–electronic coupling of the $^2\Sigma^+$ and $^2\Pi_i$ states.[7,8,40] The eigenvalues of the matrix equation for the e and f levels were then used to calculate the spin–rotation doublet splitting expected for both the perturbed and unperturbed CN $B\,^2\Sigma^+$ $v = 1$ levels. The calculation was performed using the constants of Cerny *et al.*[5] for the $X\,^2\Sigma^+$ state and the values of Ito *et al.*[8] for the $B\,^2\Sigma^+$ state. Constants for the $A\,^2\Pi_i$ levels were

Table 1 A compilation of the values of N' studied in the CN $B\,^2\Sigma^+$ $v' = 1$ level and their respective γ'_{eff} values (the error on the γ'_{eff} value is nowhere greater than $\pm 1.5\%$ of the absolute value)

N'	γ'_{eff}/cm^{-1}	N'	γ'_{eff}/cm^{-1}
4	1.730	33	1.667
6	1.718	34	1.660
7	1.719	35	1.648
9	1.706	37	1.632
10	1.701	40	1.641
11	1.708	41	1.634
13	1.749	42	1.632
14	1.754	43	1.366
15	1.724	44	1.423
16	1.736	45	1.245
18	1.736	46	7.724[a]
19	1.729	49	1.548
20	1.700	50	1.747
21	1.710	51	1.659
24	1.701	52	1.633
25	1.704	53	1.627
26	1.684	54	1.602
27	1.737	55	1.599
28	1.705	57	1.544
29	1.688	59	1.548
31	1.634	62	1.526
32	1.655	63	1.528

[a] Estimated using eqn. (2).

obtained from the coefficients of the Dunham expansion described by Kotlar *et al.*[6] and Ozaki *et al.*[7]

Fig. 5(*a*) and (*b*) show the level structure for the *e* and *f* parity levels of the $B\,^2\Sigma^+$ and $A\,^2\Pi_i$ states, respectively. The figures show the interaction of the *e* and *f* parity levels between $N' = 43$ and 49, in agreement with the results of Kotlar *et al.* If the two plots were combined, at this level of resolution, the spin–rotation doublets in the $B\,^2\Sigma^+$ state would be unresolved.

The calculated spin–rotation splitting in the $v = 1$ level of the $B\,^2\Sigma^+$ state is obtained for both the unperturbed and perturbed case. Fig. 6 shows a comparison of the experimental minus calculated splittings for both the perturbed (solid line) and unperturbed (dot-dashed line) cases. It is clear that the existing body of data for parametrising the perturbation fits the experimental observations very well. The value for the experimental minus unperturbed calculated splitting for $N' = 46$ is omitted from this plot. The difference is *ca.* 2.9 cm^{-1} with the explanation obviously related to the perturbation by the $A\,^2\Pi_i$ state.

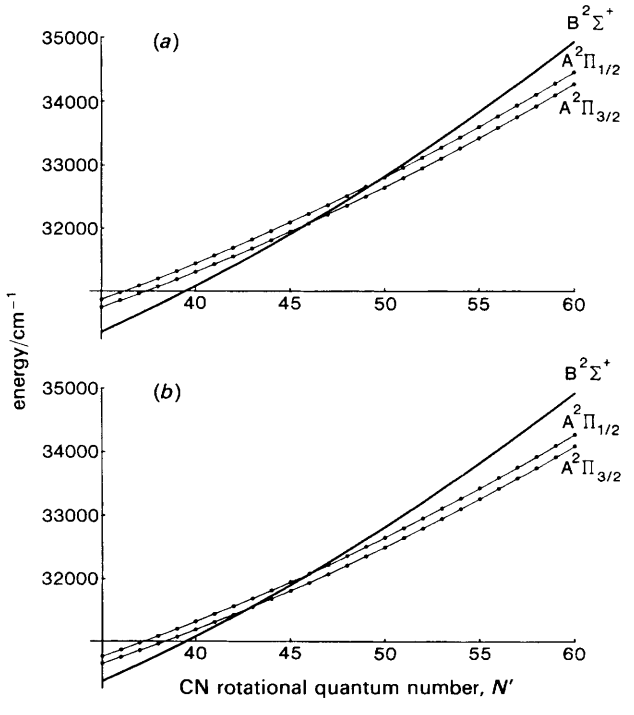

Fig. 5 Plot of the *e* parity (*a*) and *f* parity (*b*) rotational levels of the $B\,^2\Sigma^+$, $A\,^2\Pi_{1/2}$ and $A\,^2\Pi_{3/2}$ states in the region of interaction

The discrepancy for the case of the observed minus perturbed calculation, *ca.* 0.25 cm^{-1}, is harder to explain, given the excellent fit obtained for the other lines. Our lack of absolute transition frequencies precludes a rigorous reiteration of the deperturbation analysis, but a brief computational experiment varying the values of α, β and the other spectroscopic constants showed that the magnitude of the $N' = 46$ splitting was very sensitive to slight changes in the position of the rotational levels.

Discussion

It is well known that the rovibrational levels of proximate Σ and Π states may interact *via* a number of mechanisms.[1–8,40] In the specific case of $^2\Sigma$–$^2\Pi_i$ interactions, the two primary contributions to 'perturbations' come from (*a*) spin–orbit interactions and (*b*) rotation–electronic coupling.

For spin–orbit interactions, off-diagonal elements of the form

$$\langle {}^2\Pi_{1/2}, u | \boldsymbol{H}^{so} | {}^2\Sigma^+, v\rangle = \frac{a_+}{2}\langle u | v\rangle$$

(where $a_+ = \langle \pi | \hat{a} l^+ | \sigma \rangle$ is the notation of Lefebvre-Brion and Field[40] for the electronic part of the spin–orbit off-diagonal matrix element and where $\langle u | v\rangle = \delta_{uv}$ parametrises the *u*th vibrational level of the Π state and the *v*th vibrational level of the Σ state) cause a $\Delta\Omega = 0$ interaction between the $^2\Pi_{1/2}$ and $^2\Sigma^+_{1/2}$ levels. No interaction is possible involving the $^2\Pi_{3/2}$ manifold in this mechanism.

The $^2\Pi_{1/2}$ state may interact with the $^2\Sigma^+$ through rotation–electronic coupling in two ways: a $\Delta\Omega = 0$ interaction *via* an operator of the form $(1/2\mu R^2)\boldsymbol{L}^+\boldsymbol{S}^-$ (where $\boldsymbol{L}^+$ and $\boldsymbol{S}^-$ are, respectively, the raising and lowering operators of the total electronic and spin angular momentum) and a

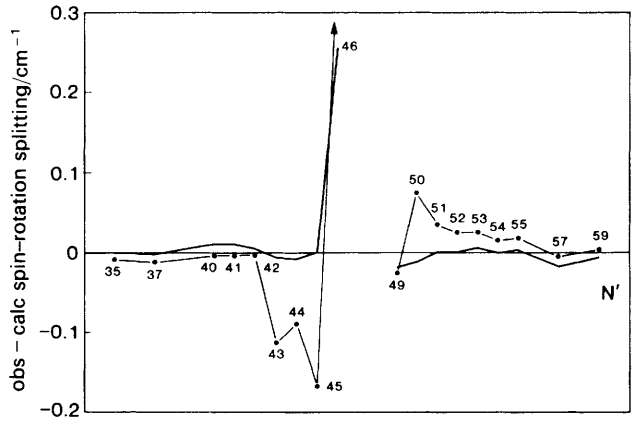

Fig. 6 Plot of the experimental minus calculated spin–rotation splitting in the perturbed region of the CN $B\,^2\Sigma^+$ ($v = 1$) rotational manifold. Shown are the calculations ignoring (– · – · –) and including (——) the effects of the $A\,^2\Pi_i$–$B\,^2\Sigma^+$ interaction. The value for $N' = 46$ ignoring the effects of the perturbation is omitted, being considerably off-scale (*ca.* 2.9 cm^{-1}). The errors on the plot, extrapolated from the errors on the measurement of γ'_{eff}, were nowhere greater than ± 0.015 cm^{-1}

$\Delta\Omega = +1$ interaction *via* terms of the form $(1/2\mu R^2)\boldsymbol{J}^-\boldsymbol{L}^+$ (where $\boldsymbol{J}^-$ is the lowering operator for total angular momentum). For the $^2\Pi_{3/2}$ manifold only the latter interaction, known as L uncoupling, is non-zero.

For each vibrational level of the $^2\Sigma^+$ state, four separate rotational levels will be perturbed by the proximate $^2\Pi_i$ manifolds. The $\Omega = \frac{1}{2}$ and $\frac{3}{2}$ manifolds will interact with distinct J levels of the $^2\Sigma^+$, *i.e.* the F_1 and F_2 levels of the level N for which $J_\Pi = J_\Sigma$.

Ito *et al.*[8] show that for the $^2\Sigma$ and $^2\Pi$ interaction of the A and B states of CN, the four interactions are close, typically spread over no more than 5–10 quanta. Our own Fig. 4 shows a cluster of interaction, centred around $N' = 46$. Kotlar *et al.*[7] give a table listing the major points of interaction of the CN $A\,^2\Pi_i$ state vibrational levels 0–15. They identify the interacting levels as $J' = 45.5$ (*e* parity, $^2\Pi_{3/2}$), $J = 42.5$ (*f* parity, $^2\Pi_{3/2}$), $J = 49.5$ (*e* parity, $^2\Pi_{1/2}$) and $J = 44.5$ (*f* parity, $^2\Pi_{1/2}$). Our data and the good fit to theory subsequently obtained corroborate this analysis.

There is one very important consequence of the $^2\Sigma$–$^2\Pi$ interaction, namely the apparent visibility of the spin–rotation splitting in the $^2\Sigma^+$ state. In the Hund's case (*b*) limit, the first-order spin–rotation Hamiltonian is given by $\boldsymbol{H}^{SR} = \gamma N \cdot S$, where γ is the spin–rotation doubling constant. In the absence of other effects, the resulting spin–rotation doubling is vanishingly small, as shown in a sample calculation by Field and Lefebvre-Brion.[40] When there are proximate Π states however, we may write[40] $\gamma_v^{obs} = \gamma_v^{true} - \rho_u^\Sigma$, where ρ_u^Σ is the second-order contribution arising from the Π state. Typically $|\rho_u^\Sigma| \gg \gamma^{true}$, and the apparent spin–rotation doubling is markedly increased, bringing it within the range of more humble spectroscopic techniques, such as that described here.

Conclusion

Sub-Doppler spectroscopy of the (1, 0) band of the CN ($B\,^2\Sigma^+$–$X\,^2\Sigma^+$) system has identified a localised perturbation, correlated to the crossing of the $B\,^2\Sigma^+$, $v = 1$ level and the $A\,^2\Pi_i$, $v = 12$ level. Fitting the Doppler profiles for a large range of N (0–60) has yielded values for an effective spin–rotation doubling constant, γ'_{eff}, which are then used to calculate experimental level separations. These have been compared with those calculated theoretically using existing spectroscopic data with excellent results.

J.F.B. thanks SERC/NATO for the award of a post-doctoral fellowship (1987–1989). We would like to thank Dr. Hanspeter Helm of SRI for the loan of an etalon for these experiments, Professor R. W. Field for supplying supplementary material to ref. 7, and John Choi for help with the figures. This work has been supported by the National Science Foundation under grant NSF-PHY 88-05603. Fig. 3 was generated using the PLT2 plotting package, written jointly by individuals at the Department of Chemistry, Harvard University, and the Cardiac Unit, Massachusetts General Hospital.

References

1 G. Herzberg, *Molecular Spectra and Molecular Structure. I. Spectra of Diatomic Molecules*, Van Nostrand Reinhold, New York, 1950.
2 J. Weinard, *Ann. Astrophys.*, 1955, **18**, 334.
3 B. Brocklehurst, G. R. Herbert, S. H. Innanen, R. M. Seel and R. W. Nichols, *Identification Atlas of Molecular Spectra. 9. The* CN $B\,^2\Sigma^+$–$X\,^2\Sigma^+$ *Violet System*, York University Centre for Research in Experimental Space Science, Toronto, 1972.
4 R. Engleman, Jr., *J. Mol. Spectrosc.*, 1974, **49**, 106.
5 D. Cerny, R. Bacis, G. Guelachvili and F. Roux, *J. Mol. Spectrosc.*, 1978, **73**, 154.
6 A. J. Kotlar, R. W. Field, J. I. Steinfeld and J. A. Coxon, *J. Mol. Spectrosc.*, 1980, **80**, 86.
7 Y. Ozaki, T. Nagata, K. Suzuki, T. Kondow and K. Kuchitsu, *Chem. Phys.*, 1983, **80**, 73.
8 H. Ito, Y. Ozaki, K. Suzuki, T. Kondow and K. Kuchitsu, *J. Mol. Spectrosc.*, 1988, **127**, 283.
9 H. Ito, K. Suzuki, T. Kondow and K. Kuchitsu, *J. Chem. Phys.*, 1991, **94**, 5353.
10 A. P. Baronavski, *Chem. Phys.*, 1982, **66**, 217.
11 W. H. Fisher, R. Eng, T. Carrington, C. H. Dugan, S. V. Filseth and C. M. Sadowski, *Chem. Phys.*, 1984, **89**, 457.
12 W. J. Marinelli, N. Sivakumar and P. L. Houston, *J. Phys. Chem.*, 1984, **88**, 6685.
13 I. Nadler, D. Mahgerefteh, H. Reisler and C. Wittig, *J. Chem. Phys.*, 1985, **82**, 3885.
14 G. E. Hall, N. Sivakumar and P. L. Houston, *J. Chem. Phys.*, 1986, **84**, 2120.
15 N. F. Scherer, J. L. Knee, D. D. Smith and A. H. Zewail, *J. Phys. Chem.*, 1985, **89**, 5141.
16 H. Joswig, M. A. O'Halloran, R. N. Zare and M. S. Child, *Faraday Discuss. Chem. Soc.*, 1986, **82**, 79.
17 M. A. O'Halloran, H. Joswig and R. N. Zare, *J. Chem. Phys.*, 1987, **87**, 303.
18 E. Hasselbrink, J. R. Waldeck and R. N. Zare, *Chem. Phys.*, 1988, **126**, 191.
19 J. F. Black, J. R. Waldeck, E. Hasselbrink and R. N. Zare, *J. Chem. Soc., Faraday Trans. 2*, 1989, **85**, 1044.
20 J. F. Black, J. R. Waldeck and R. N. Zare, *J. Chem. Phys.*, 1990, **92**, 3519.
21 J. F. Black, E. Hasselbrink, J. R. Waldeck and R. N. Zare, *Mol. Phys.*, 1990, **71**, 1143.
22 R. N. Zare, Ph.D. Thesis, Harvard University, Cambridge MA, 1964.
23 R. N. Zare and D. R. Herschbach, *Proc. IEEE*, 1963, **51**, 173.
24 J. Solomon, *J. Chem. Phys.*, 1967, **47**, 889.
25 C. Jonah, *J. Chem. Phys.*, 1971, **55**,1915.
26 R. N. Zare, *Mol. Photochem.*, 1972, **4**, 1.
27 G. E. Busch and K. R. Wilson, *J. Chem. Phys.*, 1972, **56**, 3638.
28 T. Nagata, T. Kondow, K. Kuchitsu, G. W. Loge and R. N. Zare, *Mol. Phys.*, 1983, **50**, 49.
29 R. Schmiedl, H. Dugan, W. Meier and K. H. Welge, *Z. Phys. A*, 1982, **304**, 137.
30 R. Bersohn and S. Lin, *Adv. Chem. Phys.*, 1969, **16**, 67.
31 S. Yang and R. Bersohn, *J. Chem. Phys.*, 1974, **61**, 4400.
32 S. E. Choi and R. B. Bernstein, *J. Chem. Phys.*, 1986, **85**, 150.
33 R. N. Dixon, *J. Chem. Phys.*, 1986, **85**, 1866.
34 M. Dubs, U. Brühlmann and J. R. Huber, *J. Chem. Phys.*, 1986, **84**, 3106.
35 G. E. Hall, N. Sivakumar, P. L. Houston and I. Burak, *Phys. Rev. Lett.*, 1986, **56**, 1671.
36 G. E. Hall, N. Sivakumar, D. Chawla, P. L. Houston and I. Burak, *J. Chem. Phys.*, 1988, **88**, 3682.
37 M. P. Docker, *Chem. Phys.*, 1989, **135**, 405.
38 R. N. Zare, *Angular Momentum*, Wiley, New York, 1988.
39 R. N. Zare, A. L. Schmeltekopf, D. L. Albritton and W. J. Harrop, *J. Mol. Spectrosc.*, 1973, **48**, 37.
40 H. Lefebvre-Brion and R. W. Field, *Perturbations in the Spectra of Diatomic Molecules*, Academic Press, New York, 1986.

Paper 1/05197K; *Received* 14*th October*, 1991